

Putting Density Functional Theory to the Test in Machine-Learning-Accelerated Materials Discovery

Chenru Duan^{1,2}, Fang Liu¹, Aditya Nandy^{1,2}, and Heather J. Kulik^{1,*}

¹*Department of Chemical Engineering, Massachusetts Institute of Technology, Cambridge, MA
02139*

²*Department of Chemistry, Massachusetts Institute of Technology, Cambridge, MA 02139*

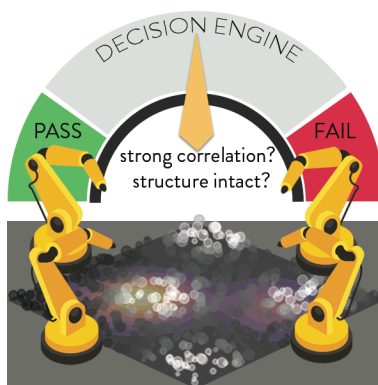
AUTHOR INFORMATION

Corresponding Author

*email: hjkulik@mit.edu, phone: 617-253-4584

ABSTRACT: Accelerated discovery with machine learning (ML) has begun to provide the advances in efficiency needed to overcome the combinatorial challenge of computational materials design. Nevertheless, ML-accelerated discovery both inherits the biases of training data derived from density functional theory (DFT) and leads to many attempted calculations that are doomed to fail. Many compelling functional materials and catalytic processes involve strained chemical bonds, open shell radicals and diradicals, or metal–organic bonds to open-shell transition-metal centers. Although promising targets, these materials present unique challenges for electronic structure methods and combinatorial challenges for their discovery. In this Perspective, we describe the advances needed in accuracy, efficiency, and approach beyond what is typical in conventional DFT-based ML workflows. These challenges have begun to be addressed through ML models trained to predict the results of multiple methods or the differences between them, enabling quantitative sensitivity analysis. For DFT to be trusted for a given data point in a high-throughput screen, it must pass a series of tests. ML models that predict the likelihood of calculation success and detect the presence of strong correlation will enable rapid diagnoses and adaptation strategies. These “decision engines” represent the first steps toward autonomous workflows that avoid the need for expert determination of the robustness of DFT-based materials discoveries.

TOC GRAPHICS



Machine learning (ML) is fast emerging as an essential complement to traditional theoretical chemistry in the accelerated discovery of molecules and materials.¹⁻³ ML models (e.g., artificial neural networks, ANNs, or kernel ridge regression, KRR) trained on appropriate representations⁴ reproduce the results calculated with electronic structure theory to within a suitable margin⁵ (ca. 1–3 kcal/mol) in challenging materials spaces such as open-shell transition-metal chemistry⁴⁻⁷ where lower-fidelity semi-empirical models fail⁸⁻¹⁰. Developments in uncertainty quantification¹¹⁻¹⁴ ensure application of these ML models only where predictions are well supported by training data. Active learning (i.e., improving ML models on the fly) has accelerated discovery¹⁵⁻¹⁸ by focusing data acquisition to the most fruitful regions of chemical space. These efforts have produced design rules and lead compounds in weeks instead of the decades that conventional high-throughput screening with density functional theory (DFT) would have required¹⁵. This scale of acceleration is most promising and most needed where traditional Edisonian efforts and intuition have failed and where search is hampered by the vastness of the combinatorial space. Transition-metal complexes exemplify this, as the range of ligands and metals along with variable oxidation and spin state of the metal create a large space for exploration, where quantum mechanical properties are difficult to predict *a priori*. These same challenges for exploration nevertheless represent opportunities or “knobs” for the design of functional materials (e.g., as switches or sensors) and selective catalysts¹⁹⁻²⁰.

Although the potential payoff for ML-accelerated discovery in challenging chemical spaces is evident, numerous obstacles remain (Figure 1). Low-cost electronic structure methods such as DFT are widely used in the generation of training data for ML models²⁻³ and in high-throughput screening²¹. By definition, ML models trained on such data sets will learn the biases of the underlying DFT functional and as a result will magnify these errors in large-scale

chemical discovery. For example, accelerated discovery of spin-crossover complexes with a model trained on semi-local DFT will only discover complexes with weaker-field ligands, whereas one trained with hybrid DFT will identify those with stronger-field ligands.²² While in small-scale studies the validity of each DFT calculation might be inspected by hand, within large-scale automated workflows^{21,23-25} manual inspection of calculation outcomes (e.g., to determine if a structure remains intact) is not possible. In addition, expert knowledge is required to determine how to accurately model systems with strong correlation²⁶⁻²⁷ or to tell when the wavefunction has converged to an unexpected (e.g., broken symmetry) result. For computational materials design²⁸ with ML¹⁻³ to deliver on its promise, we must bring expert computational chemistry knowledge into the accelerated discovery loop at the speed that ML models can deliver. In this Perspective, we describe progress towards the goal of building fully autonomous computational chemistry workflows (Figure 1). The artificial intelligence “decision engines” discussed here complement and augment expert knowledge of the computational chemist, enabling drastic increases in the size of chemical space that can be explored.

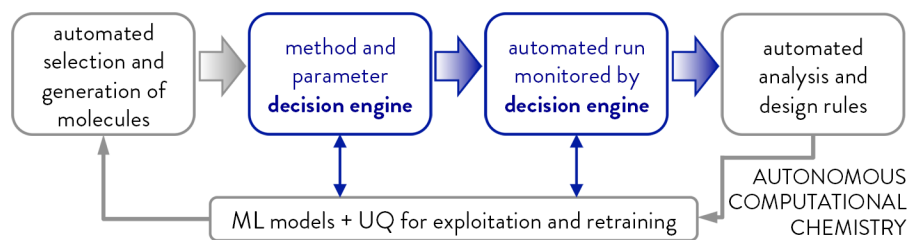


Figure 1. Schematic of the steps required in a fully autonomous computational workflow for chemical and materials discovery. The steps with widely available, established tools are shown in gray: automated selection and generation, analysis, and development of machine learning (ML) models with uncertainty quantification (UQ). The missing links for autonomous computational chemistry are shown in dark blue: artificial intelligence decision engines to select electronic structure methods and to enable monitoring of successful calculations.

A chief impediment for ML-accelerated screening of challenging chemical spaces is the high rate of failure of attempted calculations.^{7,29} For open-shell transition-metal complexes, we

classify as “failure” any of the following: changes in metal coordination number or isomer, rearrangement of atoms within or between ligands, and convergence of the wavefunction to an unexpected electronic state or with a large degree of spin contamination (Figure 2).⁷ Our heuristic definition for significant spin contamination is when deviations of the $\langle S^2 \rangle$ operator from its expected $S(S+1)$ value by greater than $1 \mu_B^2$, motivated by observations in Ref. 30 that deviations of this size led to low spin states that effectively had the properties of higher spin states in small transition metal complexes. While a computational chemist can inspect changes in structure manually and adjust the study appropriately, machine learning techniques using graph-based representations⁴ require an unambiguous chemical structure.⁷ Spin contamination and the lack of contribution from the metal center to the overall spin are also signs to a computational chemist that higher levels of theory might be needed or that a ligand is redox noninnocent³¹⁻³². ML models trained to predict spin-state-dependent properties from DFT require a more conservative filter in the data generation step to ensure the same qualitative states are being compared across the dataset.

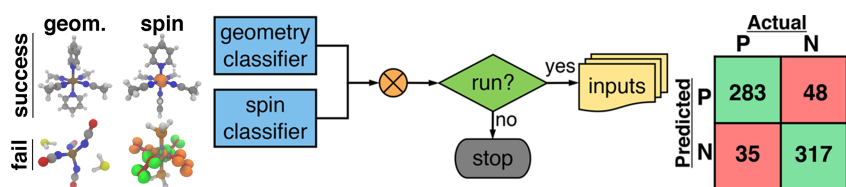


Figure 2. (Left) Examples of successful and failed calculations according to spin and geometric (geom.) classifications. (Middle) Workflow for combined spin and geometric static classifier for aborting calculations. (Right) Confusion matrix of positive (i.e., successful) and negative (i.e., failed) combined spin and geometry outcomes with a 0.5 threshold from each ANN classifier. Adapted from Ref. 29. Copyright 2019 American Chemical Society.

Compounding the challenge of calculation failure is that most optimization targets involve multiple calculations, e.g., several intermediates in a catalytic cycle as well as variable spin/oxidation state or total charge. Thus, failure of any mode of one calculation results in total loss of property evaluation. Whether in one-shot model training^{4,7,33-34} or active learning¹⁵⁻¹⁷, the

result is that less data is acquired. In a recent example¹⁵, redox couple prediction, which requires three successful geometry optimizations, saw success rates drop from 35% to 20% after five generations of active learning despite a high (50–65%) individual calculation success rate.¹⁵

Some calculation failures are foreseeable, but others are less so. A relatively free, automated combinatorial exploration of chemical space could be anticipated to produce incompatible combinations of ligands that are too highly charged, bulky, or prone to non-innocence. Still, many failures are less intuitive and may, for a given complex, depend on spin or oxidation state.²⁹ This mapping between chemistry and calculation failure is amenable to machine learning, and we trained²⁹ ANN classifiers to accurately (ca. 88–95%) predict the likelihood of calculation failures using graph-based revised autocorrelation (RAC) functions^{4,35-36} (Figure 2 and Table 1). Training a classifier to predict calculation failure based on chemical composition has the advantage that the trained model can predict success in less than a second, avoiding costly DFT calculations that are likely to fail (Figure 2). Since we observed that calculations take longer to fail than to succeed²⁹, one both avoids generating spurious data for property prediction models and most (ca. 88%) of the feasible chemical space is explored in 33% of the computational time (Table 1).²⁹

Table 1. The accuracy and area under the curve (AUC) of ANN models for geometry and spin classification tasks, as judged on the validation set used for hyperparameter selection, the set-aside test set, and an out-of-distribution set consisting of metal–oxo catalytic complexes. Adapted from Ref. 29. Copyright 2019 American Chemical Society.

Metric	Validation	Test	Oxo set
Geometry			
Accuracy	0.88	0.88	0.75
AUC	0.95	0.95	0.66
$\langle S^2 \rangle$ deviation			
Accuracy	0.95	0.96	--
AUC	0.98	0.97	--

Despite their promise, composition-derived (i.e., RAC-based) classifiers have some

limitations. Failed calculations must be intentionally generated or retained. It is wise to preserve such meta-data in high-throughput screening, as the need to anticipate how failed results bias discovery is still being understood throughout chemistry (e.g., in drug³⁷ and materials discovery³⁸⁻³⁹). However, the overhead of up-front data generation is overshadowed by the concern of transferability. Changing oxidation state and chemistry, e.g., from complexes derived from the spectrochemical series to metal-oxo species relevant for catalysis, erodes classifier performance to little better than random guess (Table 1). Uncertainty quantification based on the point's perceived (i.e., in the model latent space) distance to training data^{11,29} can be used to limit predictions to regions where the model is confident, but this will lead to predictions for a smaller fraction of the space.

We took an alternative approach, similar to recent efforts in transferable machine learning for property prediction⁴⁰⁻⁴², by noting that the electronic and geometric structures evolve during the geometry optimization. As a calculation proceeds, metrics of the geometric health of the complex⁷ (e.g., distances of ligands to the metal) or spin contamination indicate failure of a calculation, and failure or evidence of an impending failure becomes more evident with increasing numbers of steps in the optimization. A set of around 30 electronic (i.e., bond order, gradient, and partial charge) and geometric⁷ descriptors from the initial steps (ca. 2–40) of geometry optimizations were used to train convolutional neural networks (CNNs) to predict calculation failure (Figure 3).²⁹ Even for the model given the most information about optimizations, 40 steps represents only about 6 hours of GPU-accelerated calculation time⁴³ and still no more than one third of the total average time of a typical calculation.²⁹ As a demonstration of its power, we recently incorporated an extension of the dynamic classifier introduced in Ref. 29 into workflows for active learning¹⁵ of methane-to-methanol catalysts⁴⁴ in

order to reduce calculation attrition rates in catalyst discovery (Texts S1–S2, Table S1, and Figures S1–S5). The extended “dynamic” model is a multi-task network that predicts three measures of calculation health (i.e., metal spin, deviations of $\langle S^2 \rangle$ from expected values, and geometry optimization outcome) based solely on properties of the wavefunction and the energetic gradient, without explicit information about chemical composition (Figure 3). As a result, this model represents a more transferable approach⁴⁰⁻⁴² that generalizes better to new, difficult, and out-of-distribution transition-metal complexes than the “static”, compositional approach did.²⁹ From limited training data, these models efficiently avoid at least half of all failed calculations (Texts S1–S2 and Figures S2 and S5).

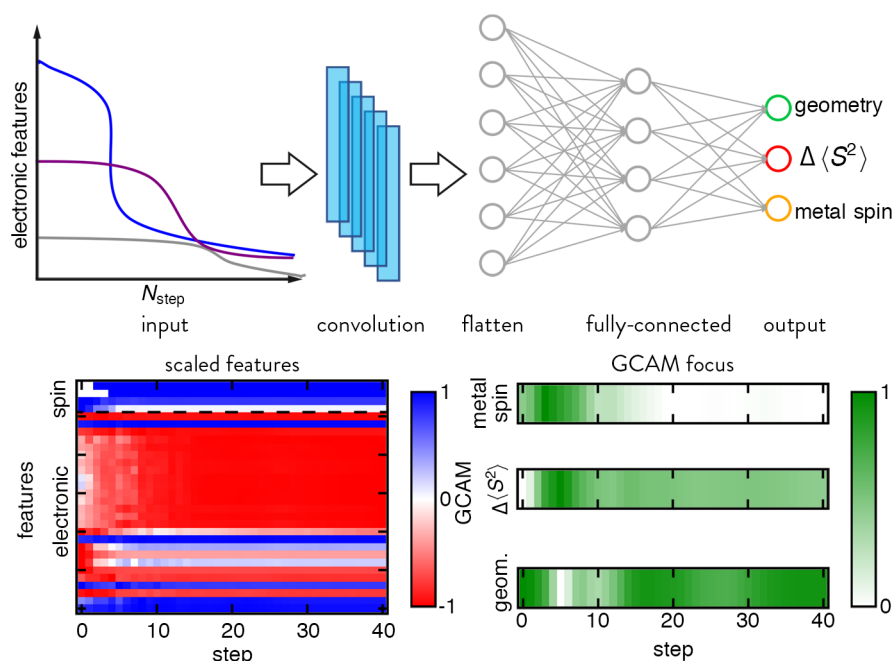


Figure 3. (top) Schematic of how electronic features are collected from the properties of the wavefunction during a geometry optimization and used as input to an ANN classifier with a convolutional layer followed by a fully connected layer. The model is a multi-task ANN classifier that predicts calculation success with respect to geometry, deviations of $\langle S^2 \rangle$ from the expected value, and the deviation of the spin on the metal from the total spin. (bottom) Gradient-weighted class-activation map (GCAM)⁴⁵ analysis of the multi-task model. In this example, the geometry optimization leads to a good result for all three properties, but features oscillate in early stages of the optimization (left). For each of the three prediction models, the GCAM focus is on different phases of the geometry optimization (right).

When paired with uncertainty quantification metrics (i.e., measured based on the latent space²⁹), the model achieves high (ca. 95–99%) accuracy by making predictions only on the complexes for which it is most confident (Figure S3). The model confidence increases with information from a greater number of optimization steps (Figure S3). CNNs can be interrogated to identify which aspect of the features have the greatest influence on predictions, for example by using a gradient-weighted class-activation map⁴⁵. With this analysis, it becomes clear why the “dynamic” approach outperforms the “static” one (Figure 3 and Figure S4). The optimizations exhibit path dependence, with some taking more or less time to fail or succeed in a manner that would be difficult to predict based on composition alone. In the future, models that use the information generated during calculations will be used to adjust calculation parameters on the fly to reduce failure rates further with dynamic control.

In ML-accelerated high-throughput screening of challenging targets (e.g., in transition-metal chemistry) with approximate electronic structure methods, it is seldom known *a priori* how the discovery process will be influenced by the choice of method. Here, approximate DFT is applied nearly exclusively, and DFT functionals that perform well for one class of materials⁴⁶ often fail to predict properties of another.⁴⁷ While it is reasonable to tailor a functional to predict properties across a narrow range of chemical space (e.g., Fe(II)/N spin-crossover complexes⁴⁶), broader discovery applications will not have experimental benchmark data or high-accuracy electronic structure results against which the optimal functional can be selected. Similarly, when traversing large regions of chemical space, one can anticipate that some regions of the space are more sensitive to method choice than others.²² Open-shell transition-metal chemistry is an example of a method-sensitive region of chemical space, where any “Jacob’s ladder” hierarchy fails⁴⁸⁻⁵¹ due to delicate trade-offs between static correlation error⁵² that is larger in hybrid

functionals⁵²⁻⁵³ and delocalization error evident in pure functionals⁵²⁻⁵⁴.

Pragmatic, low-cost approaches to addressing shortcomings of DFT or single-reference wavefunction methods are essential for high-throughput screening. Techniques relying on cancellation of errors, e.g., by adjusting between experiment and computational predictions for a reference compound⁵⁵⁻⁵⁶, cannot necessarily be guaranteed to work across the wide range of chemical compounds studied in a high-throughput screen. While not yet demonstrated for practical high-throughput screening, game theory has been proposed as a means to select⁵⁷ optimal functional/basis set pairs⁵⁸. In game theory, strategies are selected that maximize the overall benefit to multiple players. For DFT functional and basis set selection, knowledge of functional/basis set performance across a benchmark set as well as chemical similarity of a new molecule to these benchmark data was proposed as a three player problem (i.e., method accuracy, calculation complexity/cost, and chemical similarity) in game theory.⁵⁸ Sensitivity analysis and uncertainty quantification (UQ) are two complementary approaches that have been fruitfully applied in transition-metal catalysis, where the optimal electronic structure method is often unknown. Bayesian inference has been used to curate a series of DFT functionals for use in surface science⁵⁹⁻⁶⁰ by creating an ensemble of exchange-correlation functionals⁵⁹ or by using a selection of popular off-the-shelf functionals⁶⁰. For open-shell transition-metal chemistry, the fraction of Hartree–Fock (HF) exchange plays a critical role in property (e.g., spin state ordering⁶¹⁻⁶⁶) prediction. Since properties vary strongly but linearly with HF exchange, HF exchange sensitivity analysis⁶⁷ provides a useful guide to which regions of chemical space are most sensitive to functional choice²². Using ML models that predict properties at variable HF exchange fractions or that directly predict the sensitivity, we have visualized how lead compounds in large chemical spaces (e.g., over 5k spin-crossover complexes^{22,68}) change with

changing functional (Figure 4). These ML model predictions encapsulate expectations (e.g., that GGAs have a low-spin bias that favors weaker-field ligands, whereas hybrids reverse this tendency) and also highlight regions of space with properties that are relatively insensitive to functional choice (Figure 4). Given the ability of ML models to be trained on and to predict relationships between distinct functionals, one can imagine carrying out chemical discovery objectives while requiring consensus amongst functionals or methods. Although consensus does not guarantee that the electronic structure is correct, it does reduce a seldom-addressed source of uncertainty.

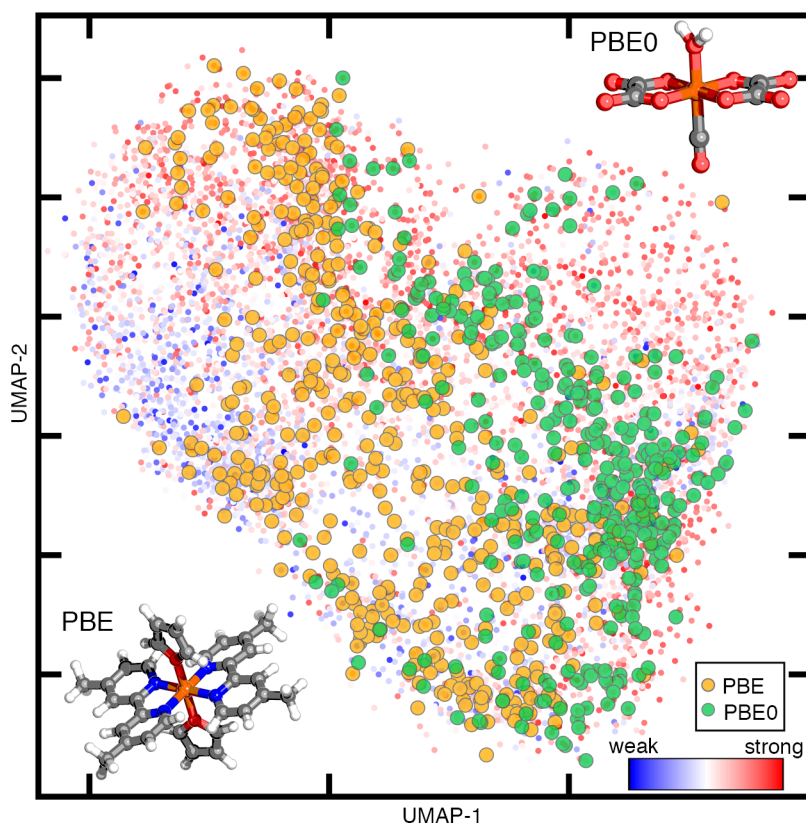


Figure 4. (top) A uniform manifold approximation and projection (UMAP)⁶⁹ visualization of a 10% random sample of 187k hypothetical complexes from Ref. ⁷⁰. Each complex (dots) is colored by a heuristic measure of ligand field strength from the average coordinating atom electronegativity (blue to red, see inset colorbar). Spin-crossover (SCO) complexes discovered by ANNs trained to predict pure GGA (PBE, in orange) or hybrid GGA (PBE0, in green) spin-splitting (i.e., ΔE_{H-L}) energies are visualized on top of this space. As in Ref. 22, an SCO is defined as $|\Delta E_{H-L}| < 2.5$ kcal/mol. Example SCOs for each functional are shown in insets:

intermediate-field Fe(III)(4,4'-dimethylbipyridine)₄(furan)₂ for PBE and a weaker-field Fe(III)(oxalate)₂(H₂O)(CO) for PBE0.

One way to sidestep the choice of DFT functional is to use higher-scaling correlated wave function theory (WFT) methods. Single-reference coupled cluster methods are the gold standard in organic chemistry. However, coupled cluster can be expected^{27,71} to perform as poorly as DFT or worse in cases where strong correlation is present. In these cases, it may be necessary to carry out time-consuming, tedious multi-reference (MR) calculations. Although some systematic approaches have been proposed⁷²⁻⁷⁴ for active space and orbital selection in MR methods, MR WFT is still too computationally demanding to apply in high-throughput screening. A number of diagnostics have been developed⁷⁵⁻⁸⁹ to probe for the presence of MR character, but they tend to disagree except in extreme cases.⁹⁰ Thus, practitioners often choose a combination of diagnostics^{26,78,91}, adjust the thresholds for diagnosing strong correlation based on material²⁶, or otherwise rely on experience to make these decisions. These less systematic behaviors can be challenging to replicate in an automated workflow.

Complicating their use in high-throughput workflows is the fact that the MR diagnostics that are highly accurate (e.g., the leading weight of the CASSCF wavefunction^{76,85-87} or amplitudes from CCSD⁷⁶⁻⁷⁸) are both high-cost and require nearly as much care as the full MR WFT calculation, making them tractable, e.g., in transition-metal chemistry, for only the smallest molecules^{26,92}. Fractional occupation number(FON)-based diagnostics from DFT provide intuitive (i.e., through spatial representations of the fractional occupation density) qualitative interpretations of MR character at low cost.^{79-80,89} Much like the HOMO–LUMO gap of a transition-metal complex^{7,93}, quantitative measures derived from finite-temperature DFT (i.e., FON-based diagnostics) can be learned by ANNs⁷⁰ trained on graph-based RAC descriptors⁴.

Interestingly, despite both quantities being derived from the placement of frontier orbitals, FON-based measures of MR character do not have a good linear correlation to HOMO–LUMO gaps (Figure 5). An advantage of training ML models to predict both quantities in chemical discovery is that we could train on a modest number of available data points, e.g., ca. 4,000 complexes from prior studies^{6-7,15,29,68}, stored in a central repository. We then predicted and visualized a much larger space (here, 187k) of hypothetical compounds to identify “DFT safe” islands, even in cases (e.g., small HOMO–LUMO gap) where one would expect DFT to fail. These methods can also be used to validate or refute expectations of imbalances in strong correlation between spin states⁹⁴⁻⁹⁵, which are more apparent for some metals (e.g., Cr(II)) than others (e.g., Fe(II)) (Figure 5).⁷⁰

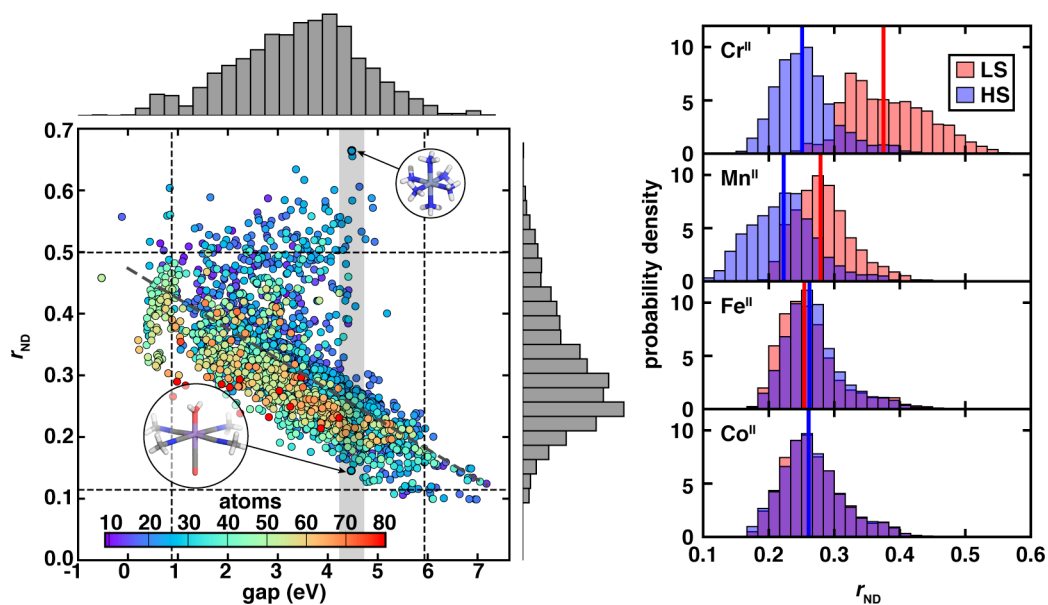


Figure 5. (left) HOMO–LUMO gap (in eV) vs r_{ND} (i.e., the ratio of non-dynamical to total correlation from FON DFT) values ($R^2 = 0.41$) for a set of over 2600 transition-metal complexes curated in Ref. ⁷⁰. Symbols are colored by number of atoms (inset colorbar), 1D histograms are shown, and dashed lines correspond to two standard deviations around the set mean. For the gray shaded region (gap around 4.5 eV), complexes with the highest (LS $\text{Cr}^{\text{II}}(\text{NH}_3)_6$) and lowest (HS $\text{Mn}^{\text{II}}(\text{misc})_4(\text{H}_2\text{O})(\text{CO})$) r_{ND} values are shown. (right) Normalized probability density distribution of r_{ND} (median shown as a vertical line) predicted by an ANN trained in Ref. ⁷⁰ on 93.6k theoretical M(II) complexes (M=Cr, Mn, Fe, Co). The translucent histograms are colored red for low-spin and blue for high-spin. Adapted from Ref. ⁷⁰. Copyright 2020 American Chemical Society.

Despite the promise of ML models to directly predict these lower-cost DFT-based diagnostics to accelerate high-throughput screening, they are not a perfect solution. The DFT-based MR diagnostics have a tendency to be less predictive of MR character than higher-cost WFT-based diagnostics (Figure 6). However, poor linear correlations between DFT-based diagnostics and the target description of strong correlation can be overcome by using ML models with lower-cost diagnostics as inputs to predict high-cost (i.e., WFT-based) diagnostics⁹⁰, similar to transfer learning^{41-42,96}. Additional motivation for such an approach comes from the observation that all diagnostics agree about the most extreme SR or MR molecules but tend to disagree about intermediate cases.^{70,90} To augment the DFT-based diagnostics, we used size-independent, structure-dependent (i.e., CD-RAC⁹⁰) chemical descriptors to encode the bonding environments that are most strongly associated with MR character. Indeed, ML (i.e., KRR) models trained on a combination of DFT diagnostics and CD-RAC descriptors accurately predict the WFT-based diagnostics at a DFT-level cost amenable to high-throughput screening (Figure 6).

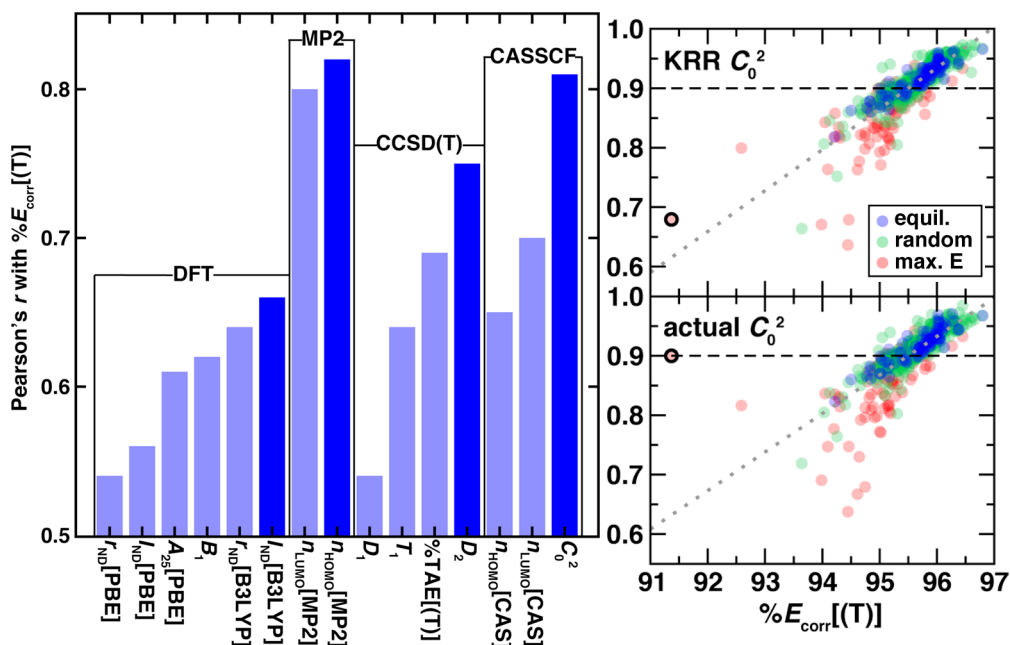


Figure 6. (left) Bar graph of unsigned Pearson's r values for percent recovery of the CCSD(T) correlation energy by CCSD, $\%E_{\text{corr}}[(T)]$, with 15 MR diagnostics over a set of 3,165 organic structures grouped by level of theory. The best-performing diagnostic is shown opaque and the remainder translucent. (right) $\%E_{\text{corr}}[(T)]$ vs actual C_0^2 (bottom) or KRR-predicted C_0^2 (top). Points are classified as equilibrium (blue circles), randomly distorted (green circles), or highest-energy (max. E, red circles) structures, and the linear correlation (dotted gray line) is computed over the complete set. A suggested MR cutoff (< 0.9) is shown as a black dashed line, and the largest KRR model error point is shown with a black outline. Adapted from Ref. ⁹⁰. Copyright 2020 American Chemical Society.

While ML models can be trained to predict higher-accuracy WFT-based diagnostics, the WFT-based diagnostics themselves still often disagree about MR character of individual molecules. For instance, cutoff-based assessments of strong correlation using MP2 occupation numbers would lead one to conclude over a set of 3,165 equilibrium and highly distorted molecules that almost none are MR, whereas excitation-based diagnostics would classify a larger fraction as MR (Figure 7). This disagreement occurs despite both diagnostics providing a good linear correlation with estimates of MR character (i.e., % recovery of the correlation energy from CCSD vs CCSD(T) or CCSDT, Figure 7).^{70,90} The picture of consensus at extreme points motivated us to use a semi-supervised machine learning approach known as virtual adversarial

training (VAT). In this approach, one trains an ANN with a modified loss function that contains both a supervised and an unsupervised term. Only the most extreme points are labeled, and the classifications of other points are learned during model training (Figure 7). VAT models are robust to noisy inputs, meaning that ML-model-predicted MR diagnostics with a small amount of noise are suitable inputs to the VAT model (Figure 7). In combination, this produces a robust “decision engine”⁷⁰ that identifies when MR character is present in a manner that can distinguish molecules where MR methods are required from those where SR methods are sufficient (Figure 7). Currently, this approach has only been trained on closed-shell CNOPS-containing small molecules, and the next step is to extend it to transition-metal complexes. Such extensions may need to exploit real-space diagnostics^{79-80,89} in conjunction with bond additivity⁹⁷ or composite⁹⁸ methods to identify and account for MR character hot spots (i.e., that could be metal- or ligand-centered).

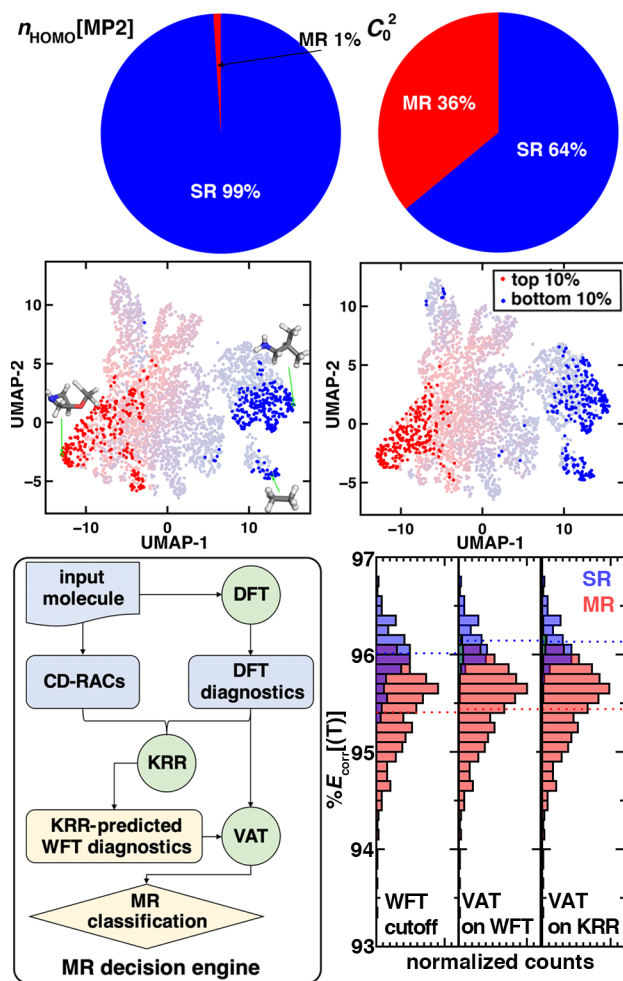


Figure 7. (top) MR/SR character of 3,165 organic structures assigned with cutoffs based on $n_{\text{HOMO}}[\text{MP2}]$ (left) and C_0^2 (right). Below each pie chart, a UMAP visualization of all 15 MR diagnostics with the structures in the top 10% (red) and bottom 10% (blue) of the relevant MR diagnostic ($n_{\text{HOMO}}[\text{MP2}]$ at left and C_0^2 at right) are shown as solid circles, with representative structures shown in inset. (bottom, left) Flowchart of the MR decision engine that combines DFT-calculated diagnostics with CD-RACs as input to KRR models to predict WFT MR diagnostics, which are used alongside DFT-calculated diagnostics as input into the VAT model for MR classification. (bottom, right) Overlapping normalized histograms of $\%E_{\text{corr}}[(T)]$ in SR (blue), transition (green), and MR (red)-classified structures shown for: classification based on a single WFT-based cutoff (left pane), VAT model from WFT and DFT-based diagnostics (middle), and VAT model on KRR-predicted WFT diagnostics (right pane). The SR and MR distributions overlap less for the VAT model than they do for the WFT cutoff model, and the two VAT models behave comparably. Adapted from Ref. ⁷⁰. Copyright 2020 American Chemical Society.

In summary, the promise of ML-accelerated materials discovery exemplified by open-shell transition-metal chemistry is matched by the challenge to move beyond the typical

accuracy, efficiency, and approach of conventional DFT-based workflows. While ML models have accelerated the discovery process, the effect of bias inherited from the training data source is not well understood. A machine learning approach similar to the one that has accelerated property prediction has been leveraged to predict quantities such as the likelihood of calculation failure or the presence of strong correlation, where chemical intuition or simpler models would fail. Once integrated into high-throughput screening workflows, these models afford improvements needed to accelerate the exploration of computationally challenging chemical spaces. While it is clear that lower level theories are in many cases not adequate for obtaining materials that achieve design objectives, it is less clear if design principles obtained from lower level theories are robust. If the design principles hold, they could be employed to accelerate materials search with higher level theories in the same spirit as transfer learning has demonstrated promise in organic chemistry.⁴¹⁻⁴² Rapid, consistent extraction of unbiased experimental reference data⁹⁹ will aid assessment of ML predictions. While challenges remain in directly applying MR methods in high-throughput workflows, developments will continue to improve their speed¹⁰⁰⁻¹⁰² and black-box nature⁷². Machine learning will contribute to improving the performance and reducing the cost of high-scaling methods to make higher-level data generation tractable for larger molecules.^{40,103-104} Once these pieces come together, fully autonomous computational chemistry will bring predictive ML-accelerated computational discovery to fruition.

ASSOCIATED CONTENT

Supporting Information. Extended description of modified dynamic classifier architecture and features, performance, and detailed analysis. (PDF)

This material is available free of charge via the Internet at <http://pubs.acs.org>.

AUTHOR INFORMATION

Notes

The authors declare no competing financial interests.

Biographies

Chenru Duan is a Ph.D. candidate in Chemistry in the group of Professor Heather J. Kulik at MIT. Prior to that, he obtained his B.S. in Physics from Zhejiang University in China in 2017.

Fang Liu is an Assistant Professor in Chemistry at Emory University. Prior to that, she did postdoctoral research in the group of Professor Heather J. Kulik at MIT (2017–2020) and obtained her Ph.D. in Chemistry at Stanford in the group of Todd J. Martínez in 2017.

Aditya Nandy is a Ph.D. candidate in Chemistry in the group of Professor Heather J. Kulik at MIT. Prior to that, he obtained his B.S. in Chemical Engineering from UC Berkeley in 2017, with a minor in Chemistry.

Heather J. Kulik is an Associate Professor in the Department of Chemical Engineering at MIT. She received her B.E. in Chemical Engineering from the Cooper Union in 2004. She obtained her Ph.D. from the Department of Materials Science and Engineering at MIT in 2009 in the group of Nicola Marzari. She completed postdocs at Lawrence Livermore with Felice Lightstone and Stanford with Todd Martínez, prior to joining MIT as a faculty member in 2013.

ACKNOWLEDGMENT

The authors acknowledge support by the Office of Naval Research under grant numbers N00014-17-1-2956, N00014-18-1-2434, and N00014-20-1-2150, DARPA grant D18AP00039, the Department of Energy under grant numbers DE-SC0018096 and DE-SC0012702, the National Science Foundation under grant numbers CBET-1704266 and CBET-1846426, and

MIT Energy Initiative seed grants (2014, 2017). H.J.K. holds a Career Award at the Scientific Interface from the Burroughs Wellcome Fund and a Marion Milligan Mason Award from the AAAS, both of which supported this work. Some of the work discussed in this Perspective made use of Department of Defense HPCMP computing resources or the Extreme Science and Engineering Discovery Environment (XSEDE), which is supported by National Science Foundation grant number ACI-1548562. The authors thank Adam H. Steeves for providing a critical reading of the manuscript.

REFERENCES

1. Dral, P. O. Quantum Chemistry in the Age of Machine Learning. *J. Phys. Chem. Lett.* **2020**, *11*, 2336-2347.
2. Janet, J. P.; Duan, C.; Nandy, A.; Liu, F.; Kulik, H. J. Navigating Transition-Metal Chemical Space: Artificial Intelligence for First-Principles Design. *Acc. Chem. Res.* **2021**, *54*, 532-545.
3. Butler, K. T.; Davies, D. W.; Cartwright, H.; Isayev, O.; Walsh, A. Machine Learning for Molecular and Materials Science. *Nature* **2018**, *559*, 547-555.
4. Janet, J. P.; Kulik, H. J. Resolving Transition Metal Chemical Space: Feature Selection for Machine Learning and Structure-Property Relationships. *The Journal of Physical Chemistry A* **2017**, *121*, 8939-8954.
5. Faber, F. A.; Hutchison, L.; Huang, B.; Gilmer, J.; Schoenholz, S. S.; Dahl, G. E.; Vinyals, O.; Kearnes, S.; Riley, P. F.; Von Lilienfeld, O. A. Prediction Errors of Molecular Machine Learning Models Lower Than Hybrid DFT Error. *J. Chem. Theory Comput.* **2017**, *13*, 5255-5264.
6. Janet, J. P.; Kulik, H. J. Predicting Electronic Structure Properties of Transition Metal Complexes with Neural Networks. *Chemical Science* **2017**, *8*, 5137-5152.
7. Nandy, A.; Duan, C.; Janet, J. P.; Gugler, S.; Kulik, H. J. Strategies and Software for Machine Learning Accelerated Discovery in Transition Metal Chemistry. *Industrial & Engineering Chemistry Research* **2018**, *57*, 13973-13986.
8. Husch, T.; Vaucher, A. C.; Reiher, M. Semiempirical Molecular Orbital Models Based on the Neglect of Diatomic Differential Overlap Approximation. *International Journal of Quantum Chemistry* **2018**, *118*, e25799.
9. Minenkov, Y.; Sharapa, D. I.; Cavallo, L. Application of Semiempirical Methods to Transition Metal Complexes: Fast Results but Hard-to-Predict Accuracy. *Journal of Chemical Theory and Computation* **2018**, *14*, 3428-3439.
10. Bannwarth, C.; Caldeweyher, E.; Ehlert, S.; Hansen, A.; Pracht, P.; Seibert, J.; Spicher, S.; Grimme, S. Extended Tight-Binding Quantum Chemistry Methods. *Wiley Interdiscip. Rev.: Comput. Mol. Sci.* **2020**, e01493.
11. Janet, J. P.; Duan, C.; Yang, T.; Nandy, A.; Kulik, H. J. A Quantitative Uncertainty Metric Controls Error in Neural Network-Driven Chemical Discovery. *Chem. Sci.* **2019**, *10*, 7913-7922.

12. Peterson, A. A.; Christensen, R.; Khorshidi, A. Addressing Uncertainty in Atomistic Machine Learning. *Phys. Chem. Chem. Phys.* **2017**, *19*, 10978-10985.
13. Musil, F.; Willatt, M. J.; Langovoy, M. A.; Ceriotti, M. Fast and Accurate Uncertainty Estimation in Chemical Machine Learning. *J. Chem. Theory Comput.* **2019**, *15*, 906-915.
14. Liu, R.; Wallqvist, A. Molecular Similarity-Based Domain Applicability Metric Efficiently Identifies out-of-Domain Compounds. *J. Chem. Inf. Model.* **2019**, *59*, 181-189.
15. Janet, J. P.; Ramesh, S.; Duan, C.; Kulik, H. J. Accurate Multiobjective Design in a Space of Millions of Transition Metal Complexes with Neural-Network-Driven Efficient Global Optimization. *ACS Cent. Sci.* **2020**, *6*, 513-524.
16. Herbol, H. C.; Hu, W.; Frazier, P.; Clancy, P.; Poloczek, M. Efficient Search of Compositional Space for Hybrid Organic–Inorganic Perovskites via Bayesian Optimization. *npj Comput. Mater.* **2018**, *4*, 51.
17. Hernández-Lobato, J. M.; Requeima, J.; Pyzer-Knapp, E. O.; Aspuru-Guzik, A. In *Parallel and Distributed Thompson Sampling for Large-Scale Accelerated Exploration of Chemical Space*, Proceedings of the 34th International Conference on Machine Learning, Proceedings of Machine Learning Research; Doina, P.; Yee Whye, T., Eds.; PMLR, Year; pp 1470-1479.
18. Tran, K.; Ulissi, Z. W. Active Learning across Intermetallics to Guide Discovery of Electrocatalysts for CO₂ Reduction and H₂ Evolution. *Nat. Catal.* **2018**, *1*, 696-703.
19. Foscatto, M.; Jensen, V. R. Automated in Silico Design of Homogeneous Catalysts. *ACS Catalysis* **2020**, *10*, 2354-2377.
20. Vogiatzis, K. D.; Polynski, M. V.; Kirkland, J. K.; Townsend, J.; Hashemi, A.; Liu, C.; Pidko, E. A. Computational Approach to Molecular Catalysis by 3d Transition Metals: Challenges and Opportunities. *Chem. Rev.* **2018**, *119*, 2453-2523.
21. Curtarolo, S.; Hart, G. L.; Nardelli, M. B.; Mingo, N.; Sanvito, S.; Levy, O. The High-Throughput Highway to Computational Materials Design. *Nat. Mater.* **2013**, *12*, 191-201.
22. Janet, J. P.; Liu, F.; Nandy, A.; Duan, C.; Yang, T.; Lin, S.; Kulik, H. J. Designing in the Face of Uncertainty: Exploiting Electronic Structure and Machine Learning Models for Discovery in Inorganic Chemistry. *Inorganic Chemistry* **2019**, *58*, 10592-10606.
23. Wang, L.-P.; McGibbon, R. T.; Pande, V. S.; Martinez, T. J. Automated Discovery and Refinement of Reactive Molecular Dynamics Pathways. *J. Chem. Theory Comput.* **2016**, *12*, 638-649.
24. Colón, Y. J.; Snurr, R. Q. High-Throughput Computational Screening of Metal–Organic Frameworks. *Chem. Soc. Rev.* **2014**, *43*, 5735-5749.
25. Wang, L.-P.; Titov, A.; McGibbon, R.; Liu, F.; Pande, V. S.; Martínez, T. J. Discovering Chemistry with an Ab Initio Nanoreactor. *Nat. Chem.* **2014**, *6*, 1044-1048.
26. Jiang, W. Y.; DeYonker, N. J.; Wilson, A. K. Multireference Character for 3d Transition-Metal-Containing Molecules. *J. Chem. Theory Comput.* **2012**, *8*, 460-468.
27. Feldt, M.; Phung, Q. M.; Pierloot, K.; Mata, R. A.; Harvey, J. N. Limits of Coupled-Cluster Calculations for Non-Heme Iron Complexes. *Journal of chemical theory and computation* **2019**, *15*, 922-937.
28. Martínez, T. J. Ab Initio Reactive Computer Aided Molecular Design. *Acc. Chem. Res.* **2017**, *50*, 652-656.
29. Duan, C.; Janet, J. P.; Liu, F.; Nandy, A.; Kulik, H. J. Learning from Failure: Predicting Electronic Structure Calculation Outcomes with Machine Learning Models. *J. Chem. Theory Comput.* **2019**, *15*, 2331-2345.

30. Ioannidis, E. I.; Kulik, H. J. Ligand-Field-Dependent Behavior of Meta-GGA Exchange in Transition-Metal Complex Spin-State Ordering. *J. Phys. Chem. A* **2017**, *121*, 874-884.
31. Kaim, W. The Shrinking World of Innocent Ligands: Conventional and Non-Conventional Redox-Active Ligands. *Eur. J. Inorg. Chem.* **2012**, *2012*, 343-348.
32. Lyaskovskyy, V.; de Bruin, B. Redox Non-Innocent Ligands: Versatile New Tools to Control Catalytic Reactions. *ACS Catal.* **2012**, *2*, 270-279.
33. Meyer, B.; Sawatlon, B.; Heinen, S.; von Lilienfeld, O. A.; Corminboeuf, C. Machine Learning Meets Volcano Plots: Computational Discovery of Cross-Coupling Catalysts. *Chem. Sci.* **2018**, *9*, 7069-7077.
34. Friederich, P.; dos Passos Gomes, G.; De Bin, R.; Aspuru-Guzik, A.; Balcells, D. Machine Learning Dihydrogen Activation in the Chemical Space Surrounding Vaska's Complex. *Chem. Sci.* **2020**, *11*, 4584-4601.
35. Virshup, A. M.; Contreras-García, J.; Wipf, P.; Yang, W.; Beratan, D. N. Stochastic Voyages into Uncharted Chemical Space Produce a Representative Library of All Possible Drug-Like Compounds. *J. Am. Chem. Soc.* **2013**, *135*, 7296-7303.
36. Moreau, G.; Broto, P. The Autocorrelation of a Topological Structure: A New Molecular Descriptor. *Nouv. J. Chim.* **1980**, *4*, 359.
37. Cáceres, E. L.; Mew, N. C.; Keiser, M. J. Adding Stochastic Negative Examples into Machine Learning Improves Molecular Bioactivity Prediction. *J. Chem. Inf. Model.* **2020**, *60*, 5957-5970.
38. Jia, X.; Lynch, A.; Huang, Y.; Danielson, M.; Lang'at, I.; Milder, A.; Ruby, A. E.; Wang, H.; Friedler, S. A.; Norquist, A. J. Anthropogenic Biases in Chemical Reaction Data Hinder Exploratory Inorganic Synthesis. *Nature* **2019**, *573*, 251-255.
39. Raccuglia, P.; Elbert, K. C.; Adler, P. D.; Falk, C.; Wenny, M. B.; Mollo, A.; Zeller, M.; Friedler, S. A.; Schrier, J.; Norquist, A. J. Machine-Learning-Assisted Materials Discovery Using Failed Experiments. *Nature* **2016**, *533*, 73-76.
40. Welborn, M.; Cheng, L.; Miller III, T. F. Transferability in Machine Learning for Electronic Structure via the Molecular Orbital Basis. *J. Chem. Theory Comput.* **2018**, *14*, 4772-4779.
41. Smith, J. S.; Nebgen, B. T.; Zubatyuk, R.; Lubbers, N.; Devereux, C.; Barros, K.; Tretiak, S.; Isayev, O.; Roitberg, A. E. Approaching Coupled Cluster Accuracy with a General-Purpose Neural Network Potential through Transfer Learning. *Nature communications* **2019**, *10*, 1-8.
42. Grambow, C. A.; Li, Y.-P.; Green, W. H. Accurate Thermochemistry with Small Data Sets: A Bond Additivity Correction and Transfer Learning Approach. *The Journal of Physical Chemistry A* **2019**, *123*, 5826-5835.
43. Seritan, S.; Bannwarth, C.; Fales, B. S.; Hohenstein, E. G.; Isborn, C. M.; Kokkila-Schumacher, S. I.; Li, X.; Liu, F.; Luehr, N.; Snyder Jr, J. W.; Song, C.; Titov, A. V.; Ufimtsev, I. S.; Wang, L.-P.; Martinez, T. J. Terachem: A Graphical Processing Unit-Accelerated Electronic Structure Package for Large-Scale Ab Initio Molecular Dynamics. *Wiley Interdiscip. Rev.: Comput. Mol. Sci.* **2020**, e1494.
44. Nandy, A.; Kulik, H. J. Why Conventional Design Rules for C-H Activation Fail for Open Shell Transition Metal Catalysts. *ACS Catal.* **2020**, *10*, 15033-15047.
45. Selvaraju, R. R.; Cogswell, M.; Das, A.; Vedantam, R.; Parikh, D.; Batra, D. In *Grad-Cam: Visual Explanations from Deep Networks via Gradient-Based Localization*, Proceedings of the IEEE international conference on computer vision, Year; pp 618-626.

46. Reiher, M.; Salomon, O.; Hess, B. A. Reparameterization of Hybrid Functionals Based on Energy Differences of States of Different Multiplicity. *Theoretical Chemistry Accounts* **2001**, *107*, 48-55.
47. Hughes, T. F.; Friesner, R. A. Correcting Systematic Errors in DFT Spin-Splitting Energetics for Transition Metal Complexes. *Journal of Chemical Theory and Computation* **2011**, *7*, 19-32.
48. Kulik, H. J. Perspective: Treating Electron over-Delocalization with the DFT+U Method. *The Journal of Chemical Physics* **2015**, *142*, 240901.
49. Furche, F.; Perdew, J. P. The Performance of Semilocal and Hybrid Density Functionals in 3d Transition-Metal Chemistry. *J. Chem. Phys.* **2006**, *124*, 044103.
50. Cramer, C. J.; Truhlar, D. G. Density Functional Theory for Transition Metals and Transition Metal Chemistry. *Physical Chemistry Chemical Physics* **2009**, *11*, 10757-10816.
51. Gaggioli, C. A.; Stoneburner, S. J.; Cramer, C. J.; Gagliardi, L. Beyond Density Functional Theory: The Multiconfigurational Approach to Model Heterogeneous Catalysis. *ACS Catalysis* **2019**, *9*, 8481-8502.
52. Duignan, T. J.; Autschbach, J. Impact of the Kohn–Sham Delocalization Error on the 4f Shell Localization and Population in Lanthanide Complexes. *J. Chem. Theory Comput.* **2016**, *12*, 3109-3121.
53. Cohen, A. J.; Mori-Sánchez, P.; Yang, W. Fractional Spins and Static Correlation Error in Density Functional Theory. *J. Chem. Phys.* **2008**, *129*, 121104.
54. Yang, X. D.; Patel, A. H.; Miranda-Quintana, R. A.; Heidar-Zadeh, F.; González-Espinoza, C. E.; Ayers, P. W. Communication: Two Types of Flat-Planes Conditions in Density Functional Theory. *J. Chem. Phys.* **2016**, *145*, 031102.
55. Konezny, S. J.; Doherty, M. D.; Luca, O. R.; Crabtree, R. H.; Soloveichik, G. L.; Batista, V. S. Reduction of Systematic Uncertainty in DFT Redox Potentials of Transition-Metal Complexes. *The Journal of Physical Chemistry C* **2012**, *116*, 6349-6356.
56. Roy, L. E.; Jakubikova, E.; Guthrie, M. G.; Batista, E. R. Calculation of One-Electron Redox Potentials Revisited. Is It Possible to Calculate Accurate Potentials with Density Functional Methods? *The Journal of Physical Chemistry A* **2009**, *113*, 6745-6750.
57. McAnanama-Brereton, S.; Waller, M. P. Rational Density Functional Selection Using Game Theory. *J. Chem. Inf. Model.* **2018**, *58*, 61-67.
58. Jensen, F. Method Calibration or Data Fitting? *Journal of chemical theory and computation* **2018**, *14*, 4651-4661.
59. Wellendorff, J.; Lundgaard, K. T.; Møgelhøj, A.; Petzold, V.; Landis, D. D.; Nørskov, J. K.; Bligaard, T.; Jacobsen, K. W. Density Functionals for Surface Science: Exchange-Correlation Model Development with Bayesian Error Estimation. *Physical Review B* **2012**, *85*, 235149.
60. Walker, E.; Ammal, S. C.; Terejanu, G. A.; Heyden, A. Uncertainty Quantification Framework Applied to the Water–Gas Shift Reaction over Pt-Based Catalysts. *The Journal of Physical Chemistry C* **2016**, *120*, 10328-10339.
61. Jensen, K. P.; Cirera, J. Accurate Computed Enthalpies of Spin Crossover in Iron and Cobalt Complexes. *The Journal of Physical Chemistry A* **2009**, *113*, 10033-10039.
62. Swart, M.; Groenhof, A. R.; Ehlers, A. W.; Lammertsma, K. Validation of Exchange–Correlation Functionals for Spin States of Iron Complexes. *The Journal of Physical Chemistry A* **2004**, *108*, 5479-5483.
63. Ganzenmüller, G.; Berkaine, N.; Fouqueau, A.; Casida, M. E.; Reiher, M. Comparison of Density Functionals for Differences between the High- (T_{2g}⁵) and Low- (A_{1g}¹) Spin States of

- Iron(II) Compounds. IV. Results for the Ferrous Complexes [Fe(L)(‘NHS4’)]. *The Journal of Chemical Physics* **2005**, *122*, 234321.
64. Droghetti, A.; Alfè, D.; Sanvito, S. Assessment of Density Functional Theory for Iron (II) Molecules across the Spin-Crossover Transition. *The Journal of chemical physics* **2012**, *137*, 124303.
65. Mortensen, S. R.; Kepp, K. P. Spin Propensities of Octahedral Complexes from Density Functional Theory. *The Journal of Physical Chemistry A* **2015**, *119*, 4041-4050.
66. Ioannidis, E. I.; Kulik, H. J. Towards Quantifying the Role of Exact Exchange in Predictions of Transition Metal Complex Properties. *The Journal of Chemical Physics* **2015**, *143*, 034104.
67. Gani, T. Z. H.; Kulik, H. J. Unifying Exchange Sensitivity in Transition Metal Spin-State Ordering and Catalysis through Bond Valence Metrics *Journal of Chemical Theory and Computation* **2017**, *13*, 5443-5457.
68. Janet, J. P.; Chan, L.; Kulik, H. J. Accelerating Chemical Discovery with Machine Learning: Simulated Evolution of Spin Crossover Complexes with an Artificial Neural Network. *J. Phys. Chem. Lett.* **2018**, *9*, 1064-1071.
69. McInnes, L.; Healy, J.; Melville, J. Umap: Uniform Manifold Approximation and Projection for Dimension Reduction. *arXiv:1802.03426* **2018**.
70. Liu, F.; Duan, C.; Kulik, H. J. Rapid Detection of Strong Correlation with Machine Learning for Transition-Metal Complex High-Throughput Screening. *The Journal of Physical Chemistry Letters* **2020**, *11*, 8067-8076.
71. Bulik, I. W.; Henderson, T. M.; Scuseria, G. E. Can Single-Reference Coupled Cluster Theory Describe Static Correlation? *J. Chem. Theory Comput.* **2015**, *11*, 3171-3179.
72. Stein, C. J.; Reiher, M. Automated Selection of Active Orbital Spaces. *Journal of chemical theory and computation* **2016**, *12*, 1760-1771.
73. Jeong, W.; Stoneburner, S. J.; King, D.; Li, R.; Walker, A.; Lindh, R.; Gagliardi, L. Automation of Active Space Selection for Multireference Methods via Machine Learning on Chemical Bond Dissociation. *J. Chem. Theory Comput.* **2020**, *16*, 2389-2399.
74. Veryazov, V.; Malmqvist, P. Å.; Roos, B. O. How to Select Active Space for Multiconfigurational Quantum Chemistry? *International Journal of Quantum Chemistry* **2011**, *111*, 3329-3338.
75. Karton, A.; Daon, S.; Martin, J. M. L. W4-11: A High-Confidence Benchmark Dataset for Computational Thermochemistry Derived from First-Principles W4 Data. *Chemical Physics Letters* **2011**, *510*, 165-178.
76. Lee, T. J.; Taylor, P. R. A Diagnostic for Determining the Quality of Single-Reference Electron Correlation Methods. *Int. J. Quantum Chem.* **1989**, *36*, 199-207.
77. Janssen, C. L.; Nielsen, I. M. B. New Diagnostics for Coupled-Cluster and Moller-Plesset Perturbation Theory. *Chemical Physics Letters* **1998**, *290*, 423-430.
78. Nielsen, I. M. B.; Janssen, C. L. Double-Substitution-Based Diagnostics for Coupled-Cluster and Moller-Plesset Perturbation Theory. *Chemical Physics Letters* **1999**, *310*, 568-576.
79. Ramos-Cordoba, E.; Salvador, P.; Matito, E. Separation of Dynamic and Nondynamic Correlation. *Physical Chemistry Chemical Physics* **2016**, *18*, 24015-24023.
80. Ramos-Cordoba, E.; Matito, E. Local Descriptors of Dynamic and Nondynamic Correlation. *Journal of Chemical Theory and Computation* **2017**, *13*, 2705-2711.
81. Kesharwani, M. K.; Sylvetsky, N.; Kohn, A.; Tew, D. P.; Martin, J. M. L. Do CCSD and Approximate CCSD-F12 Variants Converge to the Same Basis Set Limits? The Case of Atomization Energies. *Journal of Chemical Physics* **2018**, *149*, 154109.

82. Fogueri, U. R.; Kozuch, S.; Karton, A.; Martin, J. M. L. A Simple DFT-Based Diagnostic for Nondynamical Correlation. *Theoretical Chemistry Accounts* **2013**, *132*, 1291.
83. Jensen, H. J. A.; Jorgensen, P.; Ågren, H.; Olsen, J. Second-Order Moller–Plesset Perturbation Theory as a Configuration and Orbital Generator in Multiconfiguration Self-Consistent Field Calculations. *The Journal of Chemical Physics* **1988**, *88*, 3834-3839.
84. Tishchenko, O.; Zheng, J. J.; Truhlar, D. G. Multireference Model Chemistries for Thermochemical Kinetics. *Journal of Chemical Theory and Computation* **2008**, *4*, 1208-1219.
85. Sears, J. S.; Sherrill, C. D. Assessing the Performance of Density Functional Theory for the Electronic Structure of Metal-Salens: The d(2)-Metals. *J Phys Chem A* **2008**, *112*, 6741-6752.
86. Sears, J. S.; Sherrill, C. D. Assessing the Performance of Density Functional Theory for the Electronic Structure of Metal-Salens: The 3d(0)-Metals. *J Phys Chem A* **2008**, *112*, 3466-3477.
87. Langhoff, S. R.; Davidson, E. R. Configuration Interaction Calculations on the Nitrogen Molecule. *International Journal of Quantum Chemistry* **1974**, *8*, 61-72.
88. Schultz, N. E.; Zhao, Y.; Truhlar, D. G. Density Functionals for Inorganometallic and Organometallic Chemistry. *J Phys Chem A* **2005**, *109*, 11127-11143.
89. Grimme, S.; Hansen, A. A Practicable Real-Space Measure and Visualization of Static Electron-Correlation Effects. *Angew. Chem., Int. Ed.* **2015**, *54*, 12308-12313.
90. Duan, C.; Liu, F.; Nandy, A.; Kulik, H. J. Data-Driven Approaches Can Overcome the Cost-Accuracy Tradeoff in Multireference Diagnostics. *Journal of Chemical Theory and Computation* **2020**, *16*, 4373-4387.
91. Lee, T. J. Comparison of the T1 and D1 Diagnostics for Electronic Structure Theory: A New Definition for the Open-Shell D1 Diagnostic. *Chem. Phys. Lett.* **2003**, *372*, 362-367.
92. Wang, J.; Manivasagam, S.; Wilson, A. K. Multireference Character for 4d Transition Metal-Containing Molecules. *Journal of chemical theory and computation* **2015**, *11*, 5865-5872.
93. Li, Z.; Omidvar, N.; Chin, W. S.; Robb, E.; Morris, A.; Achenie, L.; Xin, H. Machine-Learning Energy Gaps of Porphyrins with Molecular Graph Representations. *J. Phys. Chem. A* **2018**, *122*, 4571-4578.
94. Flöser, B. M.; Guo, Y.; Riplinger, C.; Tuzek, F.; Neese, F. Detailed Pair Natural Orbital-Based Coupled Cluster Studies of Spin Crossover Energetics. *Journal of Chemical Theory and Computation* **2020**, *16*, 2224-2235.
95. Li Manni, G.; Alavi, A. Understanding the Mechanism Stabilizing Intermediate Spin States in Fe(II)-Porphyrin. *J. Phys. Chem. A* **2018**, *122*, 4935-4947.
96. Ramakrishnan, R.; Dral, P. O.; Rupp, M.; von Lilienfeld, O. A. Big Data Meets Quantum Chemistry Approximations: The Δ -Machine Learning Approach. *Journal of chemical theory and computation* **2015**, *11*, 2087-2096.
97. Benson, S. W.; Cruickshank, F.; Golden, D.; Haugen, G. R.; O'Neal, H. E.; Rodgers, A.; Shaw, R.; Walsh, R. Additivity Rules for the Estimation of Thermochemical Properties. *Chem. Rev.* **1969**, *69*, 279-324.
98. DeYonker, N. J.; Cundari, T. R.; Wilson, A. K. The Correlation Consistent Composite Approach (Ccca): An Alternative to the Gaussian-N Methods. *J. Chem. Phys.* **2006**, *124*, 114104.
99. Kim, E.; Huang, K.; Saunders, A.; McCallum, A.; Ceder, G.; Olivetti, E. Materials Synthesis Insights from Scientific Literature via Text Extraction and Machine Learning. *Chemistry of Materials* **2017**, *29*, 9436-9444.

100. Fales, B. S.; Curtis, E. R.; Johnson, K. G.; Lahana, D.; Seritan, S.; Wang, Y.; Weir, H.; Martínez, T. J.; Hohenstein, E. G. Performance of Coupled-Cluster Singles and Doubles on Modern Stream Processing Architectures. *J. Chem. Theory Comput.* **2020**, *16*, 4021-4028.
101. Fales, B. S.; Levine, B. G. Nanoscale Multireference Quantum Chemistry: Full Configuration Interaction on Graphical Processing Units. *J. Chem. Theory Comput.* **2015**, *11*, 4708-4716.
102. Eriksen, J. J. The Shape of Full Configuration Interaction to Come. *J. Phys. Chem. Lett.* **2020**, *12*, 418-432.
103. Brockherde, F.; Vogt, L.; Li, L.; Tuckerman, M. E.; Burke, K.; Müller, K.-R. Bypassing the Kohn-Sham Equations with Machine Learning. *Nat. Commun.* **2017**, *8*, 1-10.
104. Mills, K.; Spanner, M.; Tamblyn, I. Deep Learning and the Schrödinger Equation. *Phys. Rev. A* **2017**, *96*, 042113.